Master of Science in Mechanical Engineering

Numerical Study on the Optimal PCM Cooling Design for Pouch Cell Battery

상변화물질(PCM)을 이용한 파우치형 배터리의 냉각 최적화 수치적 연구

August 2023

Graduate School of Mechanical Engineering
Seoul National University
Ji Ho Yoo

Numerical Study on the Optimal PCM Cooling Design for Pouch Cell Battery

Advisor Min Soo Kim

Submitting a master's thesis of
Mechanical Engineering

April 2023

Graduate School of Mechanical Engineering
Seoul National University

Ji Ho Yoo

Confirming the master's thesis written by
Ji Ho Yoo

June 2023

Chair _____(Signature)
Vice Chair _____(Signature)
Examiner _____(Signature)

Abstract

In this study, the suitability and optimal design of a battery cooling system utilizing PCM was examined.

Comparing and analyzing each case's cooling performance, cooling uniformity, and power consumption while treating them– pure forced convection air cooling(PCM 0% case), hybrid cooling of air and PCM(PCM 16%, PCM 20%, PCM 28%, PCM 52% case) and pure PCM cooling(PCM 100% case)– as independent variables.

Appropriate time step, mesh size and parameters related to phase change behavior were applied for residual convergence. The numerical analysis was given reliability by adhering to numerically minimum required values for residuals. The important physical phenomenon of ‘unconstrained melting effect’ which should be implemented to accurately predict the melting behavior of PCM was also confirmed numerically.

In the interval where PCM undergoes melting, a higher content PCM case resulted in superior cooling performance compared to forced convection air cooling(PCM 0% case), primarily due to its elevated thermal conductivity, latent heat absorption during phase transition, and relatively higher heat capacity characteristic. After melting of the PCM was completed, the PCM 16% case exhibited the most efficient Cell cooling performance. Consequently, both the overall average and maximum values of Cell temperature during the cycle were observed to be the lowest in the PCM 16% case.

The application of PCM demonstrated advantages in terms of lower Cell temperature deviation and a lower Cell temperature deviation increase rate compared to forced convection air cooling in both the PCM melting interval and the post–melting interval.

Furthermore, the application of PCM confirmed its superiority in terms of power consumption compared to forced convection air cooling.

Keyword : Battery Cooling, PCM(Phase Change Material; Passive Cooling), Air(Active Cooling), Unconstrained Melting, Numerical Analysis

Student Number : 2021-28582

Table of Contents

List of Tables

List of Figures

Nomenclatures

A	Surface of control volume, m^2
A_c	Porosity function
C	Constant
C_p	Specific heat, J/kg K
D	Depth
$d\mathbf{a}$	Surface vector
dir	Direction
g	Gravitational acceleration, m/s^2
H	Total enthalpy, J/kg
H_s	Sensible enthalpy, J/kg
H_{lat}	Latent enthalpy, J/kg
k	Thermal conductivity, W/m K
L	Length
L	Latent heat, J/kg
$\dot{m}$	Mass flow rate, kg/s
p	Pressure, Pa
P_{fan}	Power consumption of fan, W
P_{AC}	Power consumption of Airconditioner, W
S	Momentum source term, m/s^2
T	Temperature, K
t	Time, s
ΔT_{air}	Temperature difference between inlet and outlet
U	Velocity vector, m/s
u	Velocity magnitude, m/s
V	Volume of control volume, m^3
$\dot{V}$	Volume flow rate, m^3/s
v_f	Velocity at the face, m/s
W	Width

Greek symbols

Γ	Diffusion coefficient
γ	Liquid fraction
ε	Constant
μ	Viscosity, N s/m^2
ρ	Density, kg/m^3
Φ	Scalar property
Δ	Difference
∇	Divergence

Subscripts

ref	Reference value
l	Liquid
s	Solid
air	Air
cell	Cell

Abbreviations

ACP	Aluminium Cooling Plate
CFD	Computational Fluid Dynamics
CFL	Courant−Friedrichs−Lewy
CMA	Cell Module Assembly
COP	Coefficient of Performance
CP	Constant Power
FVM	Finite Volume Method
HRIC	High Resolution Interface Capturing
HVAC	Heating, Venting and Air Conditioning
PCM	Phase Change Material
RSM	Response Surface Methodology

Chapter 1. Introduction

1.1. Background of study

Lithium-ion batteries have been extensively utilized due to low self-discharge rate, non-memory effects, high stability, non-memory effects, energy density, and diverse other advantages [1]. As a result, the demand for these batteries has consistently increased over time.

However, electrochemical and ohmic heating cause amount of battery heat to be produced during charging and discharging processes. If heat dissipation is not efficient, heat accumulation occurs, resulting in an increase in temperature [2-4].

The temperature rise in batteries is closely related to its lifespan and performance [5], and if proper management is not implemented, uncontrollable thermal runaway may occur [6-7].

During thermal runaway, the battery temperature can rise up to approximately 900℃, emitting substantial amounts of flammable and toxic gases [8-10], which pose significant challenges for propagation prevention and explosion suppression. Therefore, thermal management technology for batteries is essential in terms of quality and safety aspects.

Currently, active cooling using air and liquid cooling systems has been extensively applied to battery cooling. However, passive cooling utilizing phase change material(PCM) is still limited in its application due to economic constraints and cooling capacity limitations. Therefore, many researches are being conducted to enhance the marketability of cooling methods utilizing PCM.

R. Kizilel et al. [11] studied numerically to check the difference of cooling uniformity and cooling performance of passive cooling using PCM and active cooling using air through forced convection or natural convection. The study confirmed the superiority of cooling performance and uniformity in PCM cooling. Additionally, it has

been found that the PCM cooling system can prevent or delay the progress of thermal runaway. Furthermore, the PCM thermal management system was experimentally verified its ability to lower the battery pack's temperature during cycle processed. As a result, the battery capacity degradation was only at half the level compared to conventional active cooling. Consequently, the feasibility of downsizing and lightweighting in various battery applications was confirmed [12].

R. Sabbah et al. [13] numerically confirmed that active cooling using air through forced convection under severe conditions(high charge−discharge rates, high ambient temperature, high operating temperature) could not maintain the battery cell temperature below safety upper limit. However, passive cooling using PCM was able to satisfy the safety temperature requirements for battery cell temperature and demonstrated advantages in temperature uniformity of battery cells and power savings due to the absence of fan usage.

F. Chen et al. [14] numerically researched the temperature uniformity, cooling effectiveness, and cost effectiveness of three cooling methods : pure air cooling, hybrid cooling combining air and PCM, and pure PCM cooling. The variables considered were the air inlet velocity, ambient temperature, and PCM phase transition temperature. The study recommended the hybrid cooling combining air and PCM for preserving battery life and suppressing temperature variations.

Q. Li et al. [15] numerically analyzed the cooling system's design combining liquid and PCM to diminish the battery cells' peak temperature and lessen the temperature variation between the cells. The study also analyzed the difference of cooling performance according to the melting temperature variation of PCM.

In recent times, battery systems are being demanded to achieve higher energy density while reducing their overall volume through miniaturization. As a result, numerous studies are being conducted to attain the optimal cooling effect within the constraints of limited structures.

Z. Ling et al. [16] conducted an optimization study for compactness and lightweight design of hybrid cooling system for battery. The study analyzed the impact of the liquid cooling structure and PCM configuration on thermal management performance, aiming to reduce the weight and volume of PCM by using response surface methodology(RSM) and numerical PCM thermo-physical property models.

T. Tran et al. [17] confirmed that the application of flat heat pipe to battery modules resulted in an improvement of over 20% in cooling performance compared to forced convection or natural convection air cooling. Additionally, the battery cell temperature did not exceed the upper limit of 50℃. The study also demonstrated the effect of efficiently managing momentary increases in heat flux, thereby suppressing temperature fluctuations in the battery module.

For the efficient utilization of energy, the practical economic viability of cooling systems for battery systems is also being studied through a comparison of power consumption between the cooling systems.

M. Akbarzadeh et al. [18] analyzed the cooling capacity and parasitic power consumption of thermal management systems for a prismatic-shape battery module through computational fluid dynamics(CFD) simulation. Under the same power consumption, liquid cooling method exhibited a temperature approximately 3℃ lower in the hottest battery cell compared to air cooling method, and liquid cooling method also showed the improved temperature uniformity.

D. Chen et al. [19] studied cooling effects of liquid(both direct and indirect) cooling, fin cooling, and air cooling for pouch battery cells using CFD simulation based on the battery's electrochemical-thermal model. The cooling effect was evaluated based on the coolant temperature rise, the flow power consumption, and the weight of the cooling system. In air cooling, the maximum amount of parasitic power was consumed to maintain the cell temperature uniformly, while maximum temperature rise was the lowest in the indirect liquid cooling method.

In this study, pouch type battery cell currently being mass-produced by Company L was assumed as the subject of investigation.

Pouch type battery has the advantage of producing a high energy density compared to other cell types, making them promising for use as large scale batteries. Furthermore, their structural robustness has been reinforced through lamination and stacking technologies [20].

1.2. Purpose of research

Improving the cooling capacity of battery systems has the advantage of inhibiting the degradation of battery cell lifespan, thus preserving energy capacity until a later stage. This leads to operational and initial cost economy by avoiding the need for additional energy expansion or excessive initial design. Moreover, the concern about the increase in resistance due to degradation is reduced, as a result, the advantages of a cumulative effect in which heat generation within the system decreases can be expected [21].

In addition, by improving the cooling performance, compared to the existing conditions, the maximum heat dissipation load decreases. If the battery heat is accumulated in the PCM and then gradually cooled and regenerated, the peak heat dissipation load can be removed over an extended period using a smaller cooling capacity. Consequently, the required cooling capacity could be reduced, resulting to an improvement in the cost effectiveness of the cooling system [22].

In this study, the suitability and optimal design of a battery cooling system using PCM were investigated through numerical analysis. Cooling performance, cooling uniformity, and HVAC power consumption of each case—pure forced convection air cooling case, hybrid cooling of air and PCM cases, and pure PCM cooling case—were compared and analyzed by using each case as independent variables.

A PCM cooling system has the advantage of storing large amounts of energy in a compact space compared to other substances that store sensible heat. However, solely relying on PCM's latent heat cooling to refrigerate the battery system may not be sufficient to handle the battery heat generated over a period of several minutes to hours. In comparison to air cooling system, which involves a continuous supply of cold air to ensure constant heat transfer(cooling) at the interface, the cooling capacity of PCM cooling system may have limitations. Accordingly, this study aims to draw the optimal cooling system design through various case

studies combining PCM and air cooling.

Most of the previous research focused on cylindrical batteries [23, 24] or employed 2-dimensional assumptions for the review's boundary conditions [25], or the excessive application of PCM resulted in a lack of practicality [26].

The significance of this study lies in cooling the pouch type battery cells under 3-dimensional boundary conditions while maintaining the volume constraints of the actual battery system.

In dealing with phase change problems, selecting an appropriate time step, mesh size and parameters related to phase change behavior was necessary due to the energy equations at phase interfaces and rapidly changing physical properties such as viscosity and density, which can pose difficulties in achieving numerical convergence of residuals during numerical analysis. The numerical analysis was given reliability by adhering to numerically minimum required values for residuals. The important physical phenomenon of ‘unconstrained melting effect’ which should be implemented to accurately predict the melting behavior of PCM was also confirmed numerically.

Lastly, this paper aims to propose the potential utilization of PCM as a coolant by demonstrating its superiority against air cooling during battery charging and discharging processes.

Chapter 2. Numerical analysis

2.1. Physical model

As illustrated in Figure 2.1, the assembly of components such as cell, cover, busbar, cartridge, and aluminium cooling plate(ACP) is referred to as cell module assembly(CMA).

Cell is the smallest unit of battery that produces electrical power through electrochemical reactions during charging and discharging. However, heat is generated incidentally as a secondary effect due to entropy changes.

ACP plays a dual role in the cooling of each cell and supporting the cell from the front and back to counteract cell swelling occurring during charging and discharging. It serves as a micro channel for the air coolant and provides pressure support to the cell.

As shown in Figure 2.2, multiple CMAs assembled in a casing with communication cables, sensors, fuses, and other components within the casing is referred to as Pack.

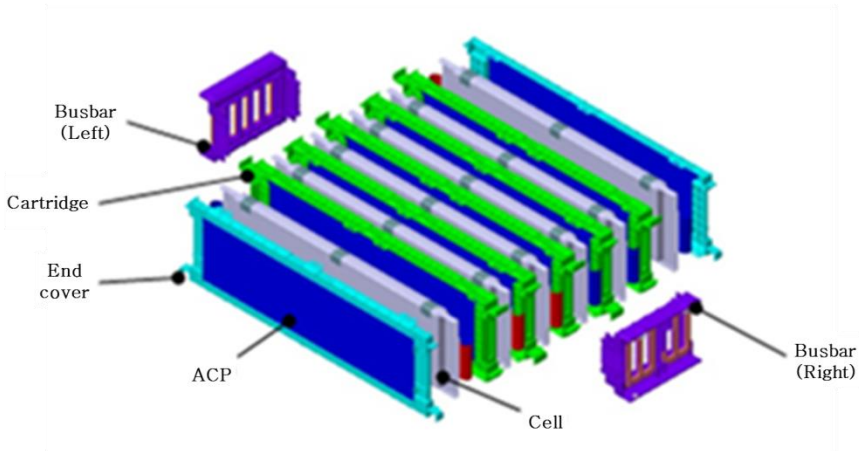

Figure 2.1 CMA parts drawing

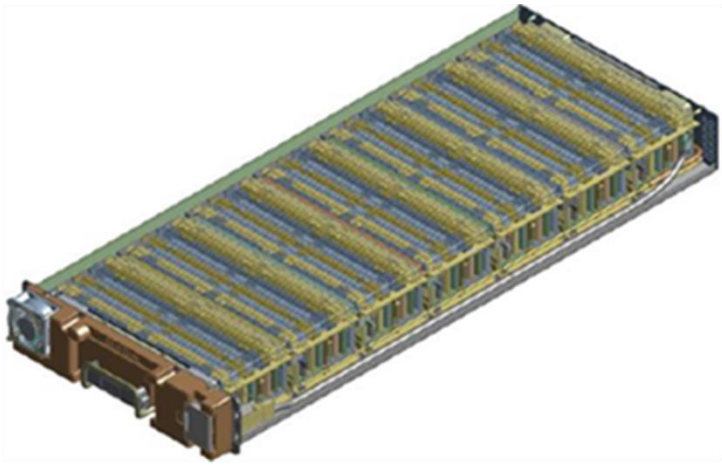

Figure 2.2 Battery pack 3D model drawing

As shown in Figure 2.3, for the purpose of optimizing the economic efficiency of the research, certain areas(Cell 4EA and ACP 5EA, central region 5 mm) capable of trend analysis were designated as the examination domain. Micro channels of the ACP, functioning as the flow channel for the air cooling, were adopted as either the air flow path or the storage slots for PCM.

Detailed dimensions are same as Figure 2.4. The study was conducted within the constraint of maintaining the actual system' s energy density by considering the sizes of real cell and ACP.

Study cases of combinations using the micro channel of ACP as storage compartments for PCM or as flow channel for air cooling were determined based on the ratio of PCM content, as depicted in Figure 2.5.

The mechanism involves heat generated by the Cell transferred to the ACP through thermal conduction and subsequently heat dissipation occurs through Air or PCM for cooling.

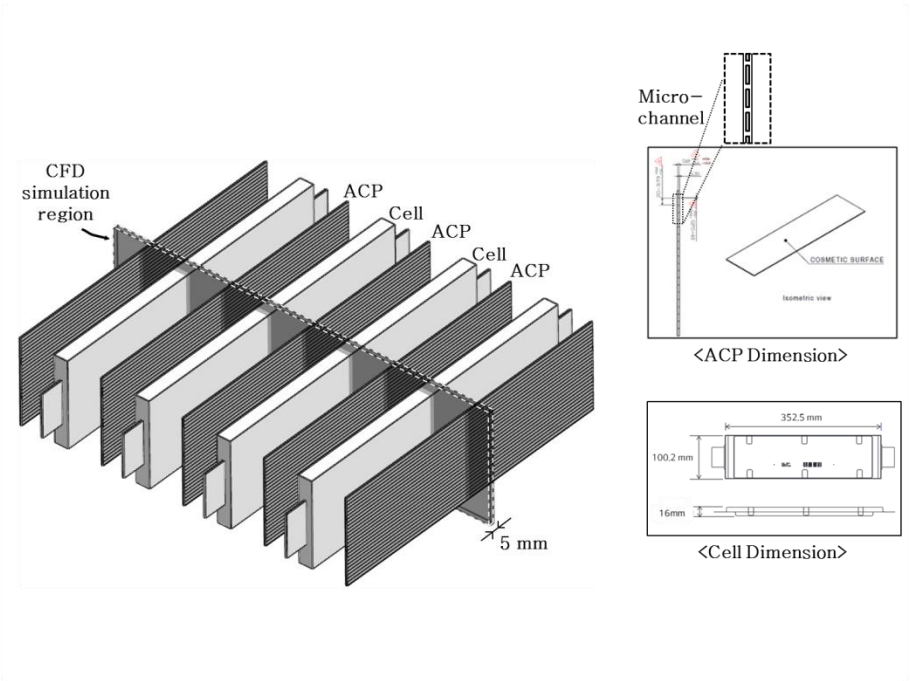

Figure 2.3 Study model schematic diagram

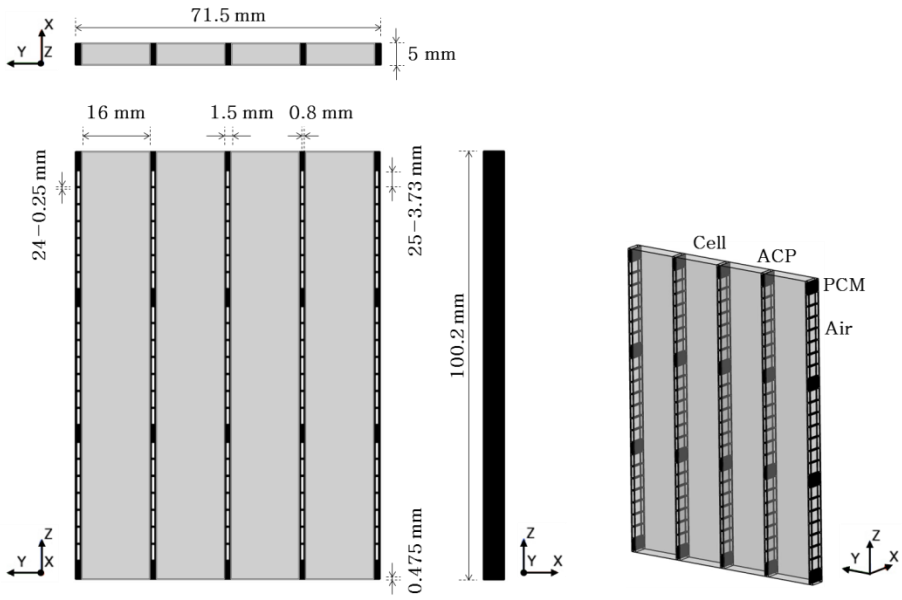

Figure 2.4 Study model detail dimension(PCM 16% case)

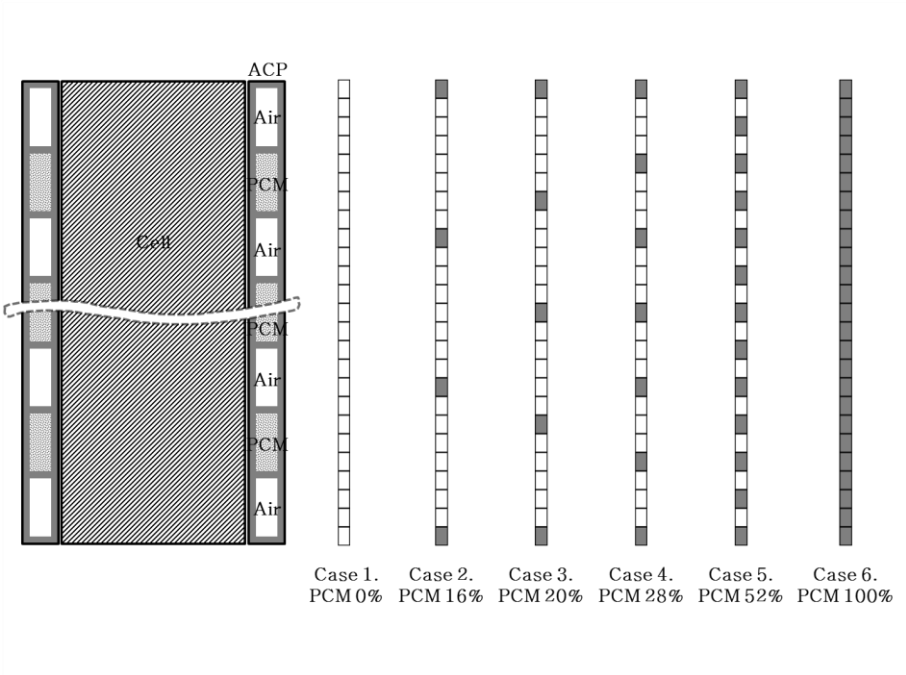

Figure 2.5 Case study illustration and comparison

The thermo-physical properties of Air, Cell and ACP applied in this study are presented in Table 1.

As for PCM, RT27(Rubitherm GmbH Co., Ltd.) was applied, which has a phase transition near the battery management temperature(298.15 K). The thermo-physical properties of the PCM are presented in Table 2.

The melting point of RT27 ranges from 301.15 K to 303.15 K, with a Mushy zone of $\Delta T = 2$ K. It was assumed that the distinct physical properties in both liquid and solid states exhibit a linear relationship within the Mushy zone.

The PCM' s thermal conductivity is diminished due to interstitial gaps between solid particles within its intrinsic crystalline structure, resulting in reduced responsiveness as a thermal management medium.

To address this issue, there have been numerous researches to enhance the thermal conductivity of PCM as a coolant such as increasing the PCM container's heat transfer rate, incorporating materials(graphite, metal foams, carbon fibers, and others) inside the container [27-30].

In this study, the PCM' s thermal conductivity was directly applied without modification. (The inter-particle contact resistance was disregarded)

The density of PCM was applied as shown in Figure 2.6.

Table 1 Thermo-physical properties of Air, Cell and ACP

Thermo-physical properties		Values
Air	Density (kg/m^3)	1.18415
	Specific heat (J/kg · K)	1,003.62
	Thermal conductivity (W/m · K)	0.02603
	Dynamic viscosity (Pa · s)	1.85508×10^{-5}
Cell	Density (kg/m^3)	2,062
	Specific heat (J/kg · K)	1,015
	Thermal conductivity (W/m · K)	25 (L, W-dir), 1.1 (D-dir)
ACP	Density (kg/m^3)	2,702
	Specific heat (J/kg · K)	903
	Thermal conductivity (W/m · K)	237

Table 2 Thermo-physical properties of PCM

Thermo-physical properties		Values
PCM	Liquidus Temperature (K)	303.15
	Solidus Temperature (K)	301.15
	Solid density (kg/m^3)	870
	Dynamic viscosity (Pa · s)	0.00342
	Liquid specific heat (J/kg · K)	1,800
	Solid specific heat (J/kg · K)	2,400
	Liquid thermal conductivity (W/m · K)	0.15
	Solid Thermal conductivity (W/m · K)	0.24
	Latent heat of fusion (J/kg)	179,000
	Thermal expansion coefficient (K^{-1})	0.0005

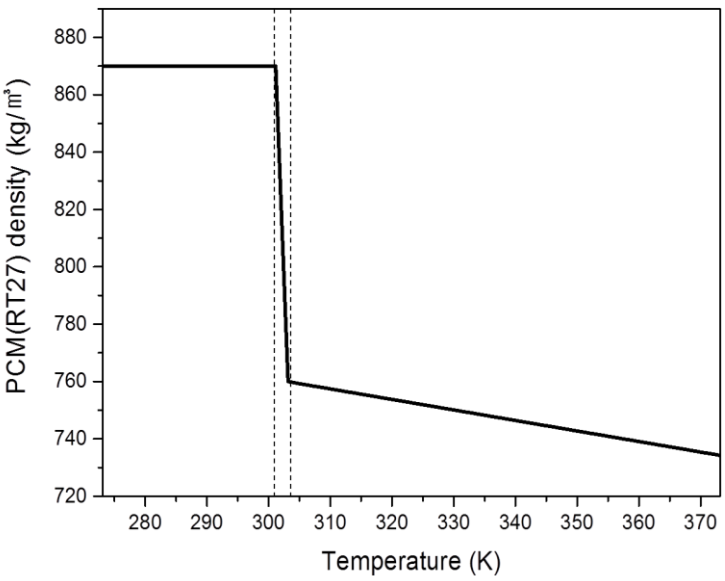

Figure 2.6 PCM(RT27) density according to the temperature

2.2. Governing equations

The 3-dimensional and unsteady governing equations applied in this study are represented by equations (1) to (5).

Continuity equation :

$$\frac{\partial \rho}{\partial t} + \nabla(\rho U) = 0 \tag{1}$$

Momentum equation :

$$\rho \frac{\partial U}{\partial t} = -\nabla p + \mu \nabla^2 U + \rho g + S \tag{2}$$

Energy equation :

$$\rho \frac{\partial H}{\partial t} = k \nabla^2 T \tag{3}$$

The S_i of equation (2) is momentum source term related to the phase change and it is expressed as follows.

$$S = -A_c(\gamma)\, u \tag{4}$$

The γ of equation (4) is the liquid volume fraction in each grid. Brent et al. [31] defined the following porosity function

$$A_c(\gamma) = \frac{C(1-\gamma)^2}{\gamma^3 + \varepsilon} \tag{5}$$

Parameter C, which determines the movement within the Mushy zone, is a parameter used to set the solid velocity to 0, and larger values result in a more rapid transition of the solid velocity to 0. Typically, values in the range of 10^4 to 10^7 are commonly employed as valid values. 10^6 was applied in this study. Forbidding division by zero, the value of ε is set to 0.001.

The enthalpy H of equation (3) equivalent to the sum of the enthalpy due to sensible heat

$$H_s = H_{ref} + \int_{T_{ref}}^{T} C_p d\,T \tag{6}$$

and the enthalpy due to latent heat

$$H_{lat} = \Upsilon L \tag{7}$$

L represents the melting process' s latent heat. In the solid state, H is 0; in the liquid state, H is L. In the Mushy zone of phase transition, H takes values between 0 and L. Therefore, Υ can be expressed as the following equation.

$$\Upsilon = \begin{cases} 0 & if\ T < T_s \\ \dfrac{T - T_s}{T_l - T_s} & if\ T_s < T < T_l \\ 1 & if\ T > T_l \end{cases} \tag{8}$$

Enthalpy method allows the application of the governing equations presented above to both liquid and solid phases uniformly, resulting in a simplified treatment of the phase change problem [32].

2.3. CFD numerical model

As a CFD simulation tool, the commercial software STAR-CCM+ 2210 Build 17.06.007 (SIEMENS Co., Ltd) was utilized for this study.

Main numerical models employed for numerical analysis in STAR-CCM+ are presented in Table 3.

The main numerical model employs the finite volume method(FVM) to find solutions within the computational domain, which is fractionized into numerous control volumes(cells) arranged in a grid-like structure(mesh). Additionally, various conservation equations in integral form are discretized and applied to each control volume to solve the problem. The values of the dependent variables, derived by solving a series of linear algebraic equations to each cell within the grid, with the number of equations matching the total number of unknowns, are stored in each respective cell. The mathematical model is transformed into algebraic equations and applied to the system, with its governing equations are discretized in both time and space.

It is possible to express all conservation equations as general transport equations, and using Gauss's divergence theorem and the general transport equations integrated over a control volume, the following integral form can be used to represent the transport equation.

$$\underbrace{\frac{d}{dt}\int_V \rho\Phi dV}_{\text{Transient term}} + \underbrace{\int_A \rho\, v_f \Phi \cdot da}_{\text{Convective flux}} = \underbrace{\int_A \Gamma\nabla\Phi da}_{\text{Diffusive flux}} + \underbrace{\int_V S_\Phi dV}_{\text{Source term}} \qquad (9)$$

· Transient term : The term representing the temporal variation of internal fluid properties inside the control volume.

· Convective flux : The term representing the convective net decrease rate of fluid properties due to convection at the boundaries of the control volume.

· Diffusive flux : The term representing the diffusive net increase rate of fluid properties due to diffusion at the boundaries of the control volume.

· Source term : The term representing the formation or dissipation of fluid properties within the control volume.

Once Φ is applied to variables such as 1, velocity, work, energy, enthalpy, and appropriate diffusion coefficient Γ and source term are selected, it is possible to derive conservation equations for mass, momentum, and energy in the form of partial differential equations.

Table 3 Numerical models for analysis(SIEMENS [33])

Numerical model 1. Eulerian Multiphase Segregated Flow (for continuity and momentum equation) Remark • Distinct conservation equations are solved for each phase. • Each phase is treated as a continuum can penetrate each other and each phase shares the common pressure field. (Example : Dispersed[bubbles/droplets], Large interface[resolved free surfaces], Symmetric/Mixed[no clear distinction])
Numerical model 2. Volume of Fluid(VOF) Remark • Solves a set of conservation equations and an additional volume fraction equation. • Between immiscible fluids, it traces the free surface. • Simulation of the advection transport of immiscible fluid by using high resolution interface capturing(HRIC) scheme. • Phase change process : evaporation and condensation, boiling, gas dissolution, melting and solidification.
Numerical model 3. Melting and Solidification Remark • It can consider the effect of phase transition on the energy equation. • The thermo-physical properties are applied according to solid fraction. • Fluid flow can be stopped when the solid fraction excesses specific value through a subsection 'Flow Stop' model.
Numerical model 4. Mushy Zone Permeability Remark • A Mushy Zone is a stationary area that has partially solidified and is interspersed with dendrites. • Flow resistance of Mushy zone can be reflected by using 'Carman-Kozeny Mushy Zone Permeability' model.
Numerical model 5. Segregated Multiphase Temperature (for energy equation) Remark • Energy equation for the entire multiphase flow region is calculated so that enthalpy of PCM according to the temperature can be decided.
Numerical model 6. Reynolds-Averaged Navier-Stokes (for Turbulence effects) Remark • For the Reynolds-Averaged Navier-Stokes equations, it can furnish closure relations for the mean flow quantity transport. • The RANS equations are obtained by decomposing every variable within the instantaneous Navier-Stokes equations into its average value and its turbulent fluctuation component.
Numerical model 7. K-Epsilon Turbulence (for Turbulence effects) Remark • It is based on RANS model, and to calculate the turbulent eddy viscosity, a two-equation model is used to calculate transport equations governing turbulent dissipation rate and turbulent kinetic energy [34].

2.4. Boundary and initial conditions

Airflows for each study case were computed through steady state CFD simulations at the system level, as shown in Figure 2.7.

Performance curve of the axial fan utilized in the simulation is presented in Figure 2.8.

The slots containing PCM are enclosed at the front and back of the micro channel, thereby fully trapping the PCM inside the ACP structure.

Consequently, as the PCM content increased, the airflow was decreased due to the reduced flow path, leading to an increase in system resistance and a reduction in air flow, as shown in Table 4.

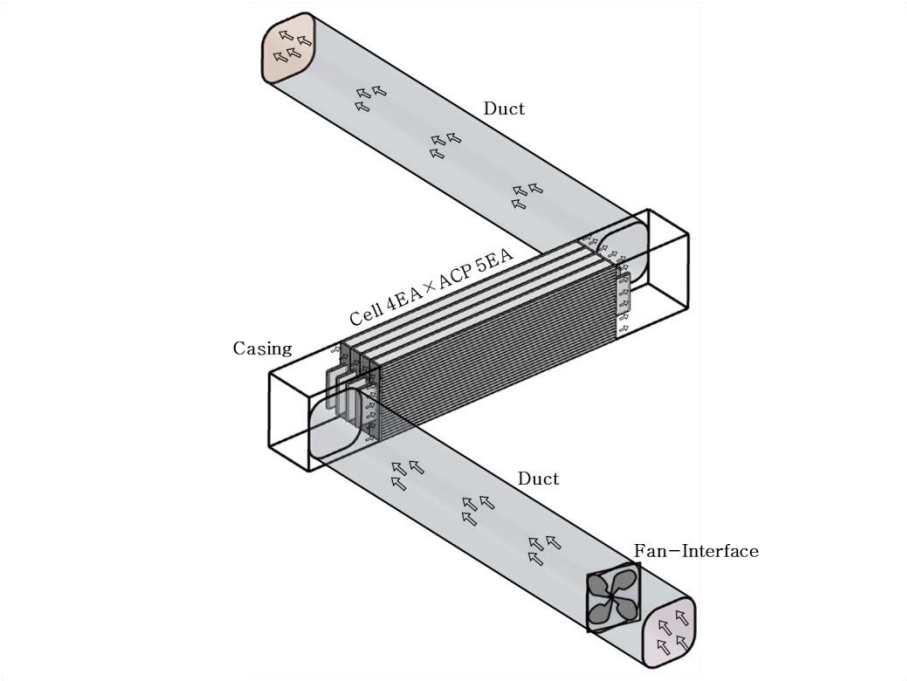

Figure 2.7 System level flow analysis schematic diagram

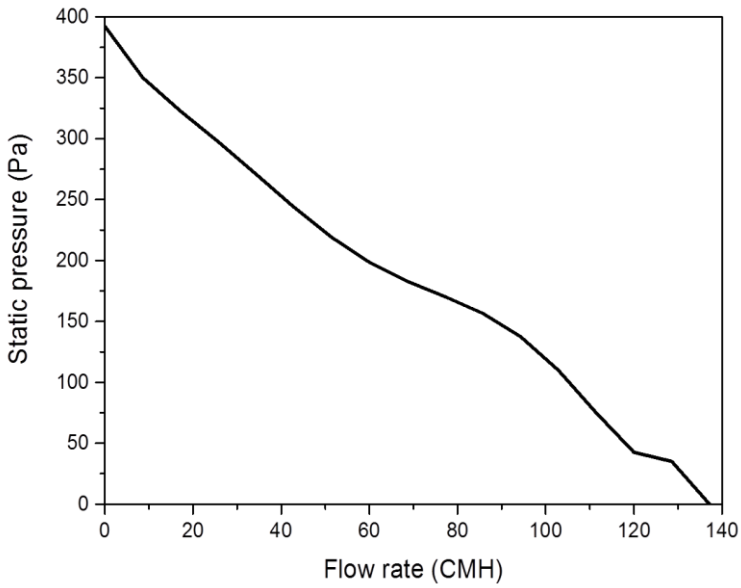

Figure 2.8 Fan performance curve for system level flow analysis

Table 4 System level flow analysis results

Case	Outlet flow rate (kg/s)	Pressure drop (Pa)
PCM 0%	0.00100	377.4
PCM 16%	0.00085	379.0
PCM 20%	0.00081	379.5
PCM 28%	0.00073	380.2
PCM 52%	0.00049	383.8
PCM 100%	–	–

The heat generation of the Cell was set to 15.09W, corresponding to the average heat generation of 1CP cycle.

Adiabatic conditions were applied to the Cell's upper, lower, front, back, and ACP outer surfaces, as well as the front and back surfaces of the PCM. Interfaces between each region were designed to have no contact resistance, allowing for mutual heat transfer to occur.

The Air region assumed a flow from front to rear as depicted in Figure 2.9, and to apply fully developed flow, the ‘Fully developed interface’ condition was applied to inlet and outlet surfaces.

It was presumed that the initial temperature of all regions was 300.15 K. Additionally, it was assumed that there is sufficient cooling capacity to refrigerate the dissipated heat, and as a result, it was expected that air would always be supplied to the Air region's inlet boundary at a temperature of 300.15 K.

The effect of radiative heat transfer between the regions was disregarded.

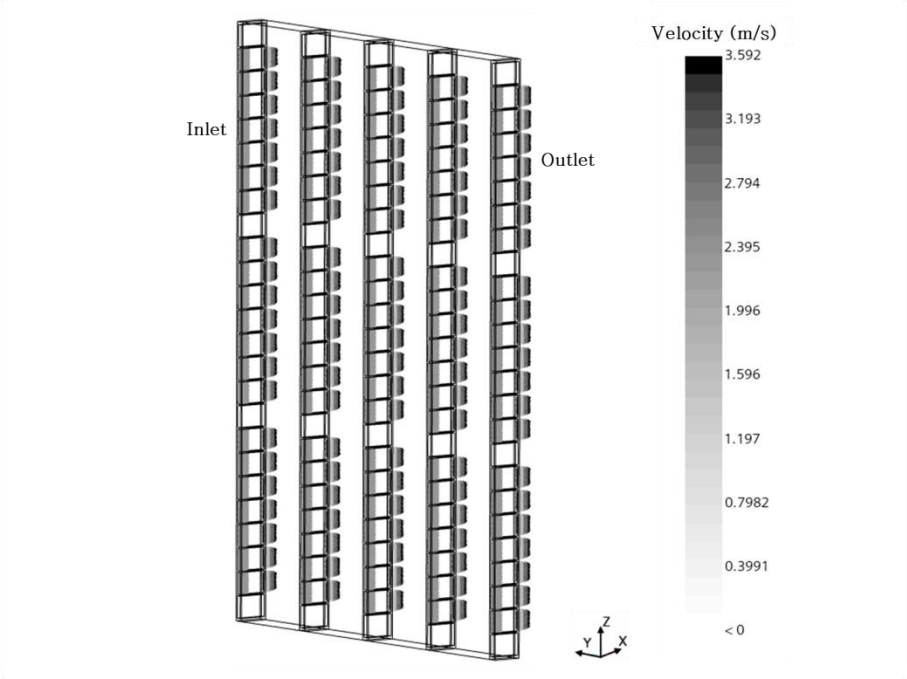

Figure 2.9 Velocity vector of Air region(PCM 16% case)

2.5. Numerical solution controls

In dealing with phase change problems, the energy equation at the phase interface is mathematically nonlinear, which means that exact solutions exist only in specific cases involving numerous assumptions. For most cases, approximate or numerical methods are used for solving the problem.

The suitability of each physical equation was pursued by applying the minimum residual value criterion, as presented in Table 5, to achieve confidence in the analysis results.

Table 5 Residual values criteria

Criterion	Minimum required values
Continuity	10^{-10}
x, y, z−momentum	10^{-9}
Energy	10^{-6}

2.6. Time step and grid independence study

To ensure the numerical convergence stability, time step was set to 0.0005 seconds, allowing the CFL number to remain below a certain level(approximately 10).

For the system level flow analysis to determine the air flow rate for each study case, as shown in Figure 2.10, once the number of meshes in the Air region exceeded approximately 51.4 million, there was no longer any variations in the outlet flow rate value. Therefore, the mesh specification was configured at the corresponding level.

Air region where forced convection occurs was expected to experience significant flow resistance and frequent changes in flow direction within the casing. Therefore, as depicted in Figure 2.11, to accurately model turbulent flow, a polyhedral mesh, suitable for simulating turbulent flow phenomena, was employed. To consider the influence of viscosity on the flow, a thin and dense grid layer called a prism layer mesh was applied to the boundary surface of the Air region adjacent to the ACP region surface.

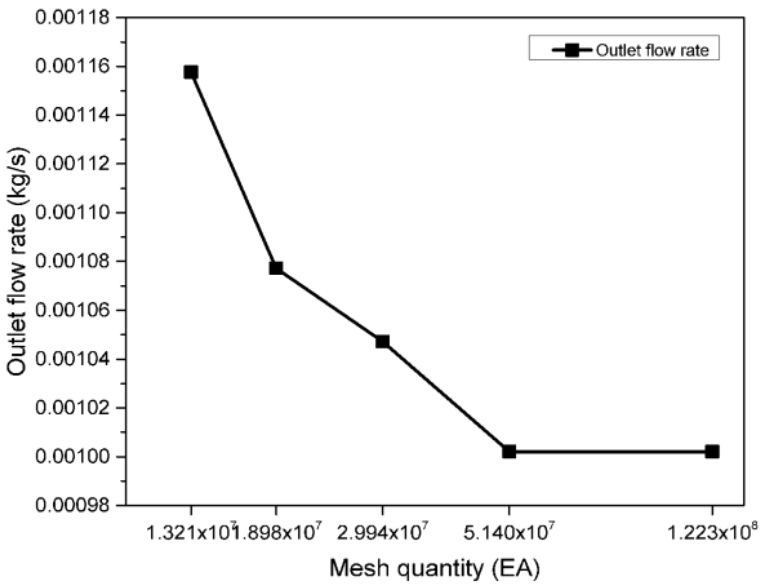

Figure 2.10 Grid independence study results(system level flow analysis)

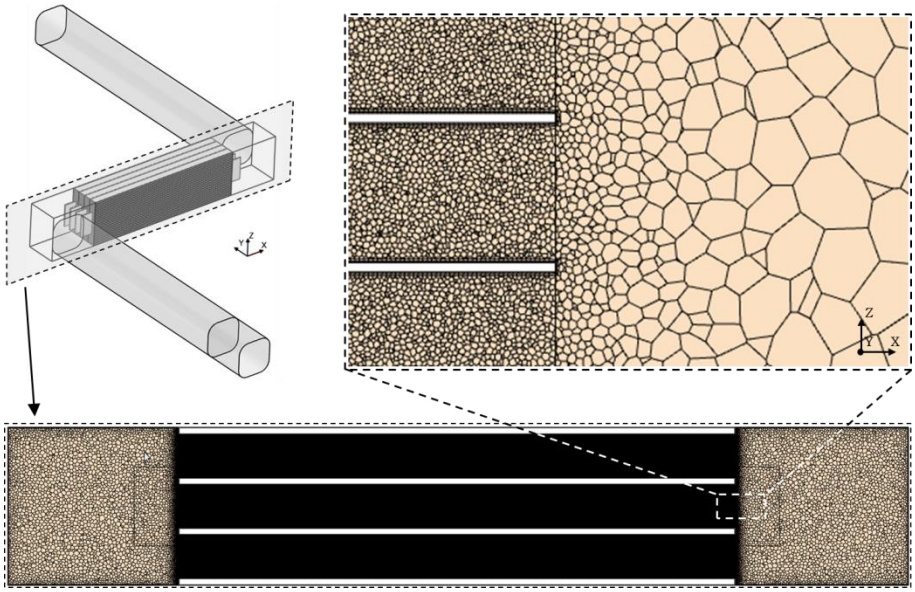

Figure 2.11 Mesh configuration of system level flow analysis(PCM 16% case)

In the cooling analysis of the PCM and air combination, the mesh size(0.05 mm, 0.07 mm, 0.10 mm, and 0.20 mm) of the PCM region was considered as a independent variable, and the changes in Cell temperature and PCM solid fraction under specific conditions were investigated as dependent variables. As shown in Figure 2.12, once the size of the mesh is smaller than 0.10 mm, the change behavior of physical quantities tends to be saturated. Therefore, the mesh size of the PCM region was selected to be 0.07 mm.

As shown in Figure 2.13, a cuboid-shaped trimmer mesh was utilized for the solid region(Cell, ACP) where heat transfer occurs solely through conduction and for the Air region with a uniform square cross-section duct, in which only unidirectional flow exists in the longitudinal direction. A polyhedral mesh was utilized for the PCM region, where intricate natural convection flows occur due to density differences. To consider the influence of viscosity on the flow, a thin and dense grid layer called a prism layer mesh was used for the boundary surface of the Air and PCM region adjacent to the ACP region surface.

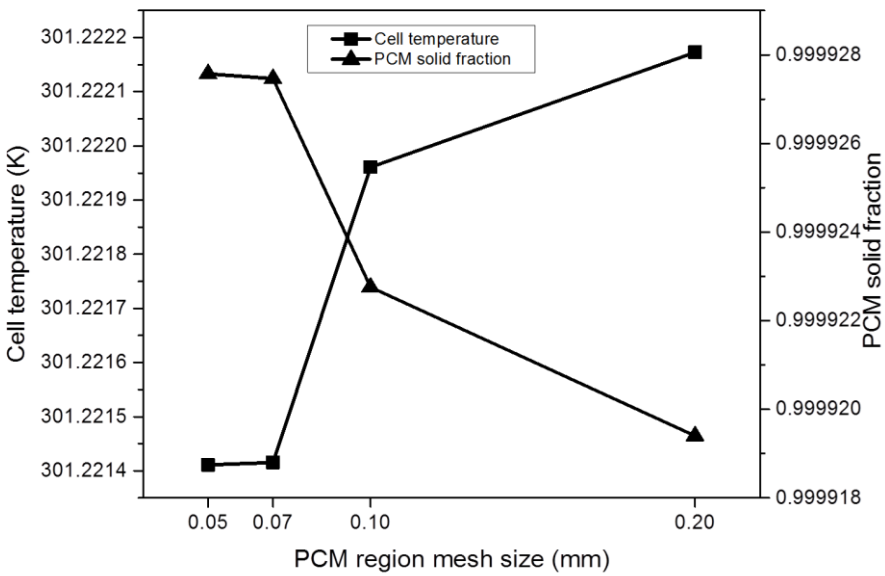

Figure 2.12 Grid independence study results(cooling analysis)

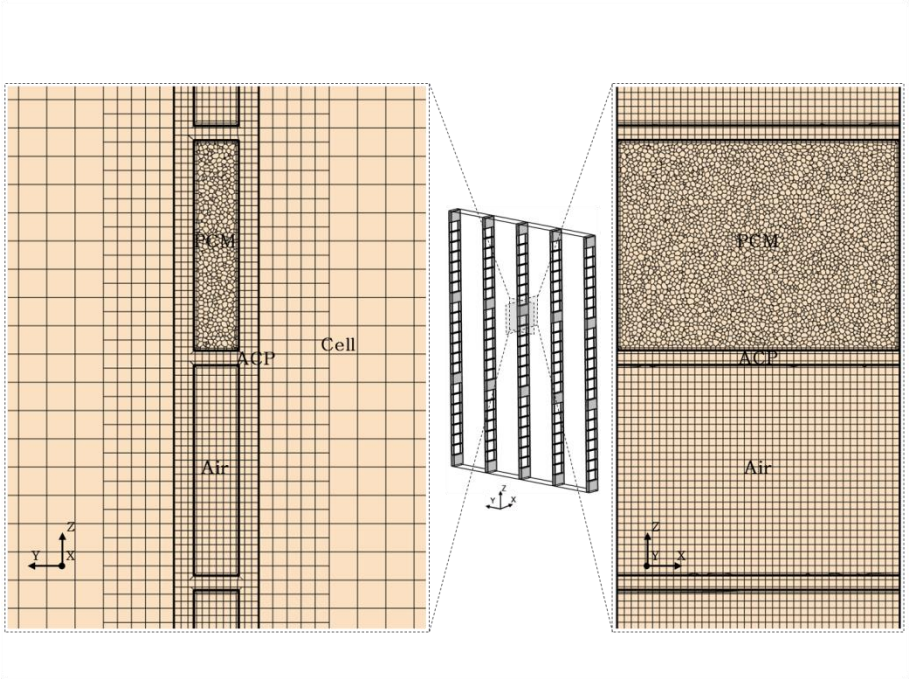

Figure 2.13 Mesh configuration of cooling analysis(PCM 16% case)

2.7. Validation

Solid PCM inside the container settles downward due to its relatively higher density. Until the solid PCM completely melts, it precipitates downward but does not make complete contact with the bottom surface of the container. The solid PCM remains suspended, maintaining fine gaps, due to the pressure exerted by the fluid in the gap located between the bottom surface of the container and the solid PCM. At this moment, an intense heat conduction phenomenon occurs through the fluid in the gap located between the bottom surface of the container and the solid PCM. As a consequence, the rate of phase transition accelerates more rapidly compared to when the solid PCM is not settled beneath the container. This phenomenon is denoted as the 'Unconstrained melting effect' considering the density variation of PCM. It is an important physical phenomenon to be implemented to accurately predict the melting behavior of PCM [35].

F. L. Tan [36] compared the experimental results of PCM melting inside a spherical capsule with the analytic solutions. As shown in Figure 2.14, the rate of phase change of PCM within a spherical capsule is approximately 55.6% faster due to the unconstrained melting effect compared to the case of constrained melting.

In this study, it was considered that the phase change behavior of PCM was adequately implemented by observing the phenomenon of unstrained melting through the spatial behavior of PCM melting in each study case, as shown in Figure 2.15.

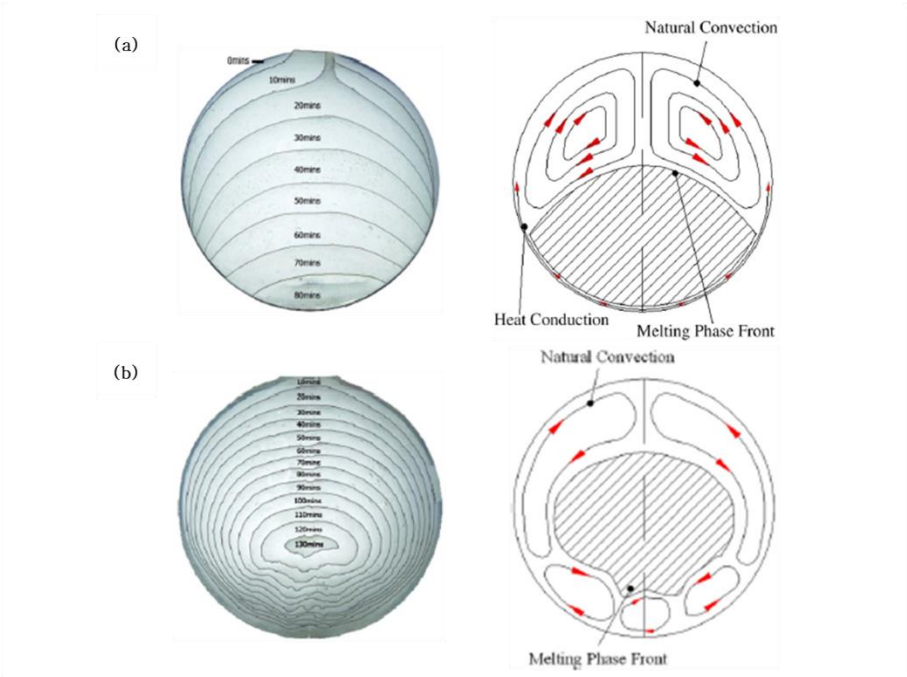

Figure 2.14 Experiment results and conceptual streamline
(a) Unconstrained melting (b) Constrained melting(F. L. Tan [36])

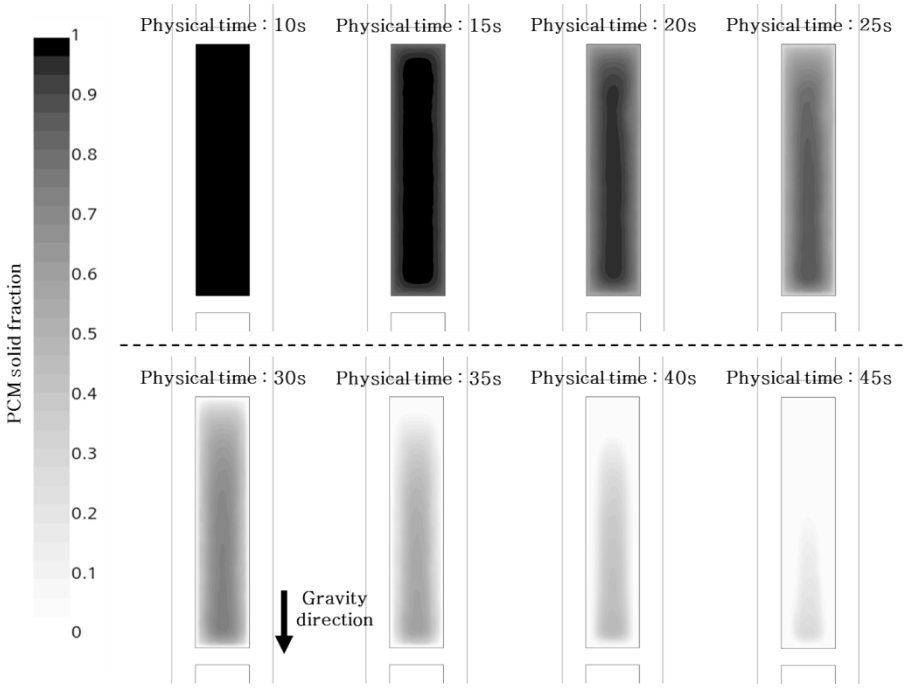

Figure 2.15 PCM solid fraction distribution of PCM 16% case

For validation purposes, the two phenomena were numerically compared by assuming specific boundary conditions, as a result, as shown in Figure 2.16, the distinct differentiation between the behaviors of PCM's unconstrained melting and constrained melting allowed for the confirmation of the suitability of the analysis model.

Due to the geometrical characteristics [37] of the microchannel with a large aspect ratio and relatively high heat transfer conditions compared to the PCM content, the phase change rates between the two phenomena exhibited an approximate 9.3% difference, as depicted in Figure 2.17. This resulted in somewhat quantitative discrepancies compared to previous studies.

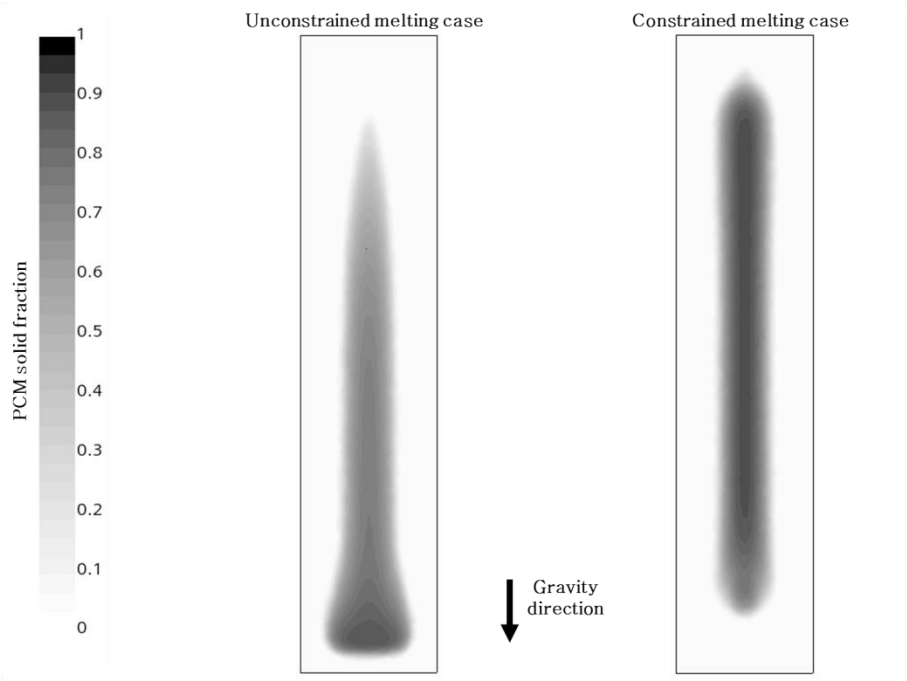

Figure 2.16 Difference in progress : unconstrained melting(left) and constrained melting(right)

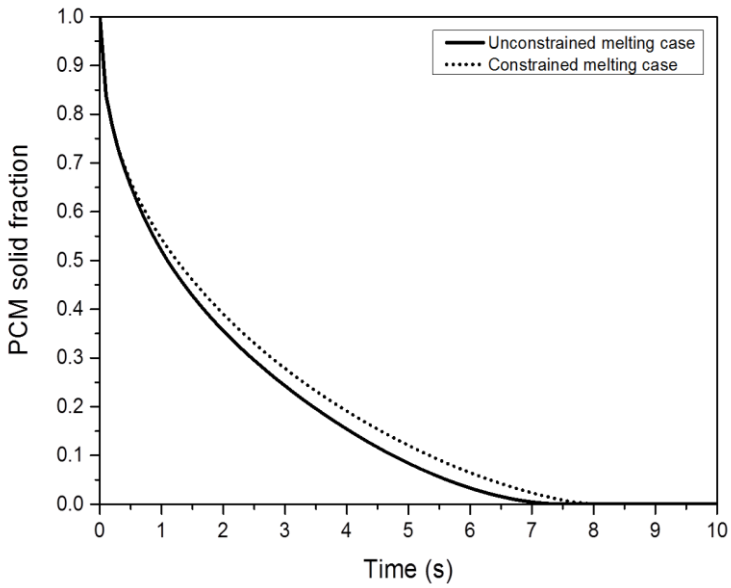

Figure 2.17 Difference in pace of PCM solid fraction change

Chapter 3. Results and discussion

3.1. Case study results

3.1.1. Progress of PCM melting

As shown in Figure 3.1 and Figure 3.2, melting of PCM initiates in all cases at around 11 seconds. Melting starts earlier and ends earlier for cases with lower PCM content. Despite assuming a relatively high heat generation for the battery, it seems difficult to control the battery's temperature throughout the entire cycle by relying exclusively on the latent heat absorption that occurs during PCM melting. If excessive heat accumulates in the PCM for a prolonged period after melting, the PCM may lose its temperature control effectiveness. Consequently, to dissipate the heat, it will be necessary to integrate alternative cooling models.

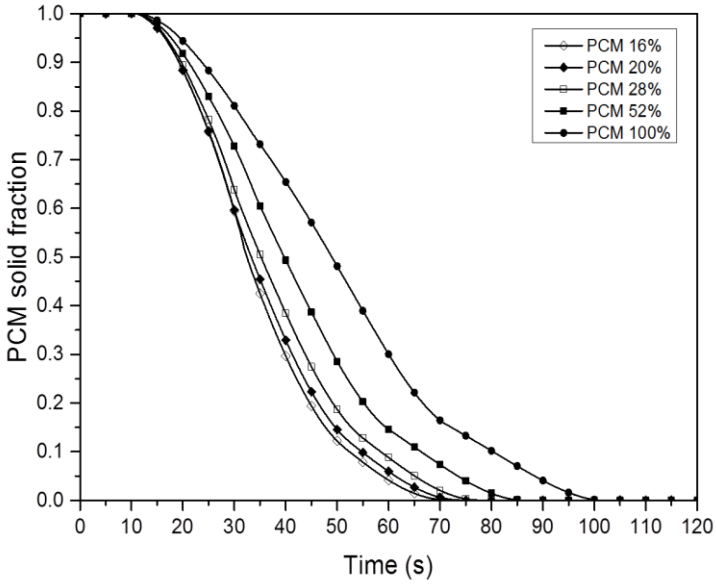

Figure 3.1 PCM solid fraction behavior

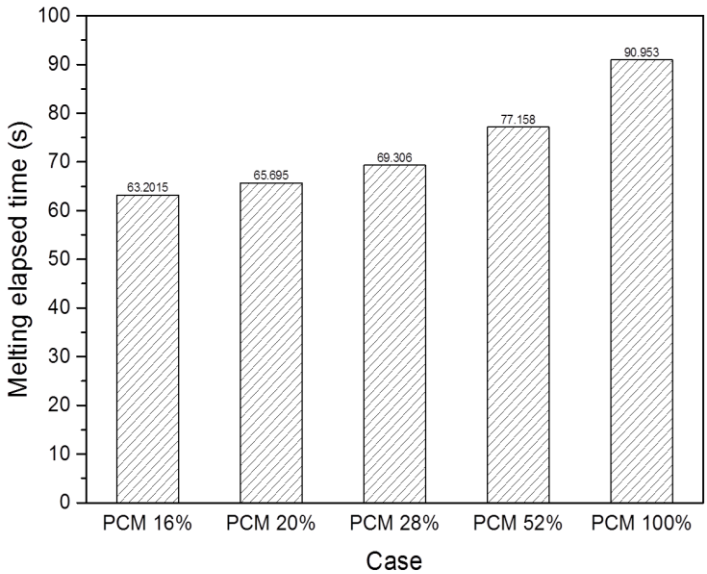

Figure 3.2 PCM melting elapsed time

3.1.2. Cell temperature[①]

In the interval of 0 to 120 seconds, where cooling is manifested due to PCM melting, there is an observed trend that cases with higher proportions of PCM exhibit lower average and maximum cell temperatures throughout the cycle, as shown in Figure 3.3, Table 6, Figure 3.4. This phenomenon is considered as a result of rapid heat transfer through conduction to the PCM, latent heat absorption during phase transition of the PCM, and the relatively large heat capacity of the PCM.

However, after about 105 seconds when the PCM melting in all cases was totally completed, the Cell temperature increased more in cases with a higher PCM content, except for air cooling case(PCM 0% case), as shown in Figure 3.5, Table 7.

① It is the volume average temperature of the four cells.

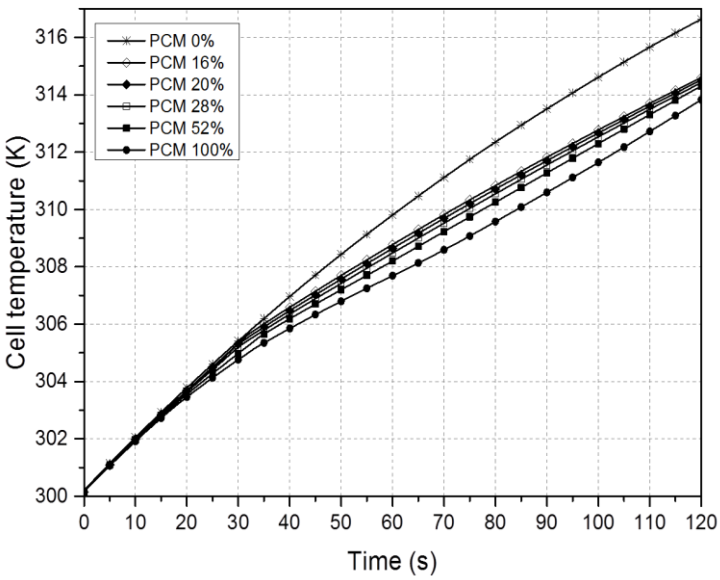

Figure 3.3 Cell temperature behavior(time : 0~120 s)

Table 6 Cell temperature results(time : 0−120 s)

Case / Time: 0−120 s	PCM 0%	PCM 16%	PCM 20%	PCM 28%	PCM 52%	PCM 100%
Average value (K)	309.35	308.37	308.28	308.17	307.98	307.56
Rate of change against air cooling (PCM 0% case) (%)	−	−10.7	−11.6	−12.8	−14.9	−19.5
Maximum value (K)	316.64	314.60	314.51	314.42	314.31	313.83
Rate of change against air cooling (PCM 0% case) (%)	−	−12.4	−12.9	−13.5	−14.1	−17.0

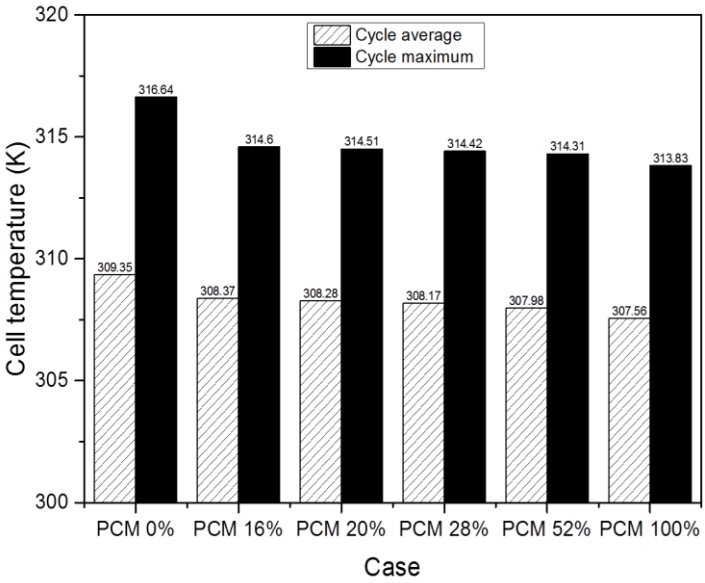

Figure 3.4 Cycle average and maximum Cell temperature(time : 0-120 s)

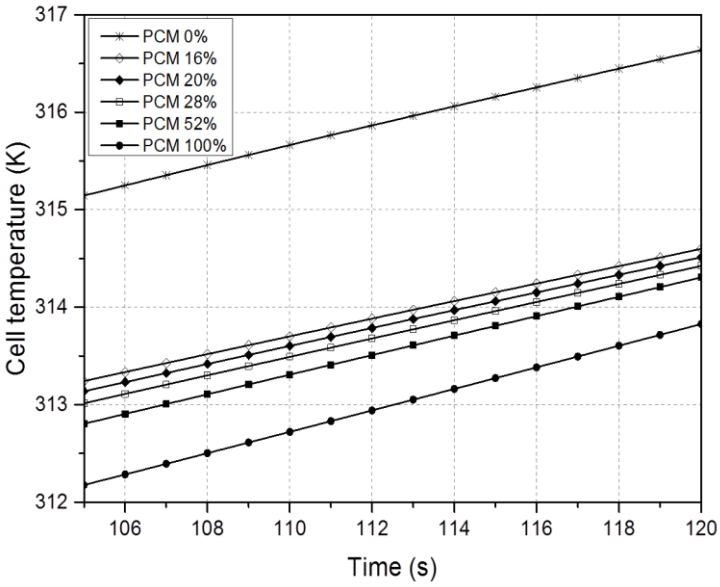

Figure 3.5 Cell temperature increase rate after melting(time : 105−120 s)

Table 7 Cell temperature increase rate(time : 105−120 s)

Case / Time: 105−120 s	PCM 0%	PCM 16%	PCM 20%	PCM 28%	PCM 52%	PCM 100%
Cell temperature increase rate (K/s)	0.0996	0.0904	0.0917	0.0939	0.1001	0.1101

As the Cell’s heat generation was assumed to be equivalent to that of a 1CP cycle(1 hour charging and discharging), the Cell temperature between 120 and 3,600 seconds was estimated(extrapolation) using a fitted logarithmic equation obtained through nonlinear regression analysis based on the Cell temperature between 0 and 120 seconds, as shown in Table 8.

Consequently, considering all intervals of the 1CP cycle comprehensively, both the average and maximum values of Cell temperature were calculated in the order of PCM 16% < PCM 20% < PCM 28% < PCM 52% < PCM 0% < PCM 100% case, indicating that the cooling capacity of the hybrid cooling of air and PCM method(PCM 16% case) was the most superior, as shown in Figure 3.6, Table 9, Figure 3.7.

Although Cell cooling occurs through latent heat absorption during PCM melting, there was no observed deceleration in Cell temperature rise or reduction in Cell temperature. This phenomenon is considered as a consequence of rapid accumulation of heat due to the conservative application of heat generation and heat dissipation performance limits.

Table 8 Estimated equations for Cell temperature(time : 120−3,600 s)

Case	Estimated regression equation	Coefficient of determination
PCM 0%	T_{cell} = 11.173 × ln(time) + 263.144	0.9999
PCM 16%	T_{cell} = 10.154 × ln(time) + 265.975	
PCM 20%	T_{cell} = 10.299 × ln(time) + 265.196	0.9998
PCM 28%	T_{cell} = 10.553 × ln(time) + 263.892	
PCM 52%	T_{cell} = 11.244 × ln(time) + 260.460	
PCM 100%	T_{cell} = 12.372 × ln(time) + 254.576	0.9995

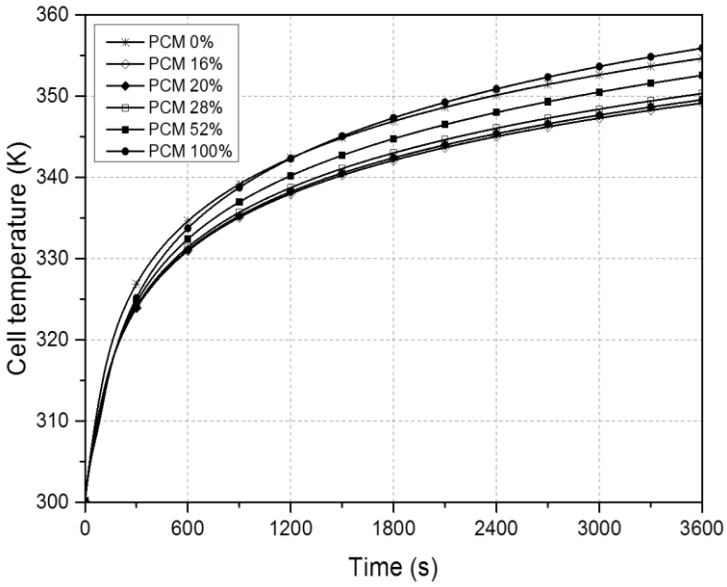

Figure 3.6 Cell temperature behavior(time : 0−3,600 s)

Table 9 Cell temperature results (time : 0−3,600 s)

Case / Time: 0−3,600 s	PCM 0%	PCM 16%	PCM 20%	PCM 28%	PCM 52%	PCM 100%
Average value (K)	343.59	339.10	339.37	339.89	341.45	343.72
Rate of change against air cooling (PCM 0% case) (%)	−	−10.3	−9.7	−8.5	−4.9	+0.3
Maximum value (K)	354.64	349.13	349.53	350.31	352.54	355.89
Rate of change against air cooling (PCM 0% case) (%)	−	−10.1	−9.4	−7.9	−3.9	+2.3

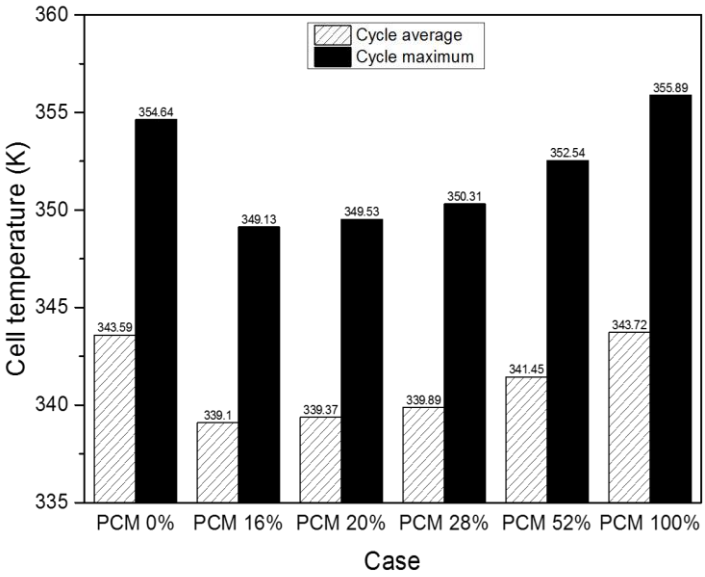

Figure 3.7 Cycle average and maximum Cell temperature(time : 0−3,600 s)

3.1.3. Cell temperature deviation[②]

The Cell temperature deviation frequently changed its ranking among the cases during the 0 to 120 seconds period, and except for the air cooling case(PCM 0% case), there was a tendency after 120 seconds that was difficult to predict with a specific correlation equation, as listed in Figure 3.8.

The Cell temperature deviation observed at the 120 seconds through CFD simulation is presented in Table 10.

Each case shows an inflection point in the trend of Cell temperature deviation near the time when PCM is completely melted. After the inflection point, as shown in Table 11, the increase in Cell temperature deviation was smaller in cases with a higher PCM content. This phenomenon is considered as a consequence of the rapid heat diffusion through conduction with a higher PCM content, resulting in reduction in spatial temperature imbalances.

[②] It is the temperature difference between the four cells with the highest and lowest temperature. (Temperature deviation in spatial distribution)

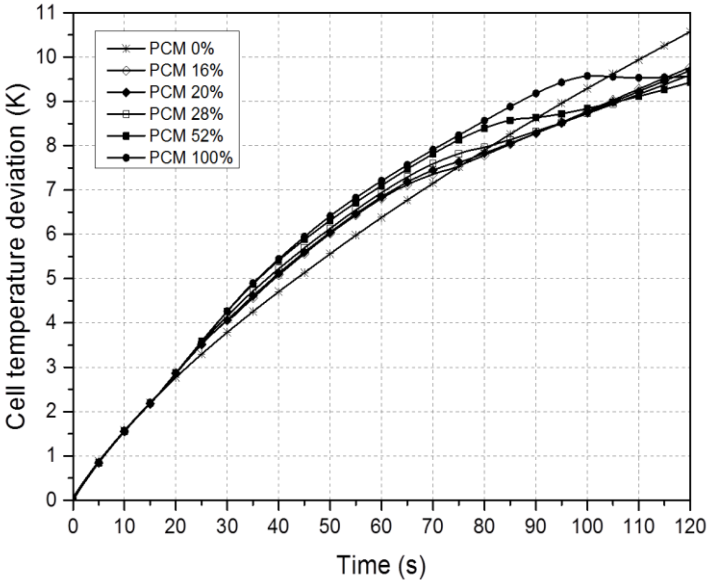

Figure 3.8 Cell temperature deviation behavior(time : 0−120 s)

Table 10 Cell temperature deviation(time : 120 s)

Case / Time: 120 s	PCM 0%	PCM 16%	PCM 20%	PCM 28%	PCM 52%	PCM 100%
Cell temperature deviation (K)	10.57	9.77	9.70	9.60	9.43	9.57

Table 11 Cell temperature deviation increase rate(time : 105−120 s)

Case / Time: 105−120 s	PCM 0%	PCM 16%	PCM 20%	PCM 28%	PCM 52%	PCM 100%
Cell temperature deviation increase rate (K/s)	0.0634	0.0493	0.0473	0.0436	0.0304	0.0009

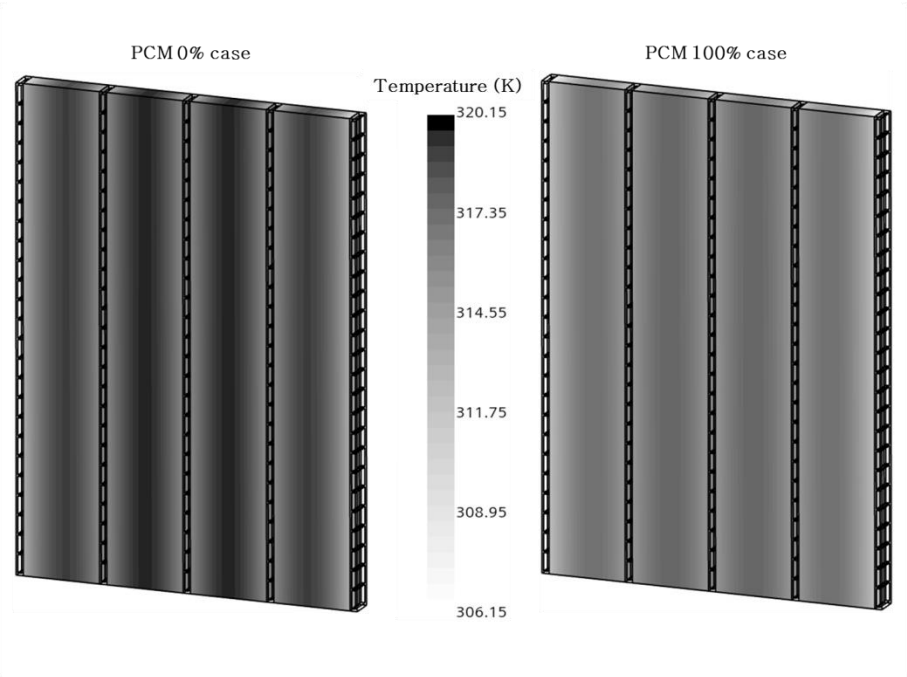

Figure 3.9 Cell temperature distribution(PCM 0% and PCM 100% case)

3.1.4. HVAC power consumption

Chen et al. [14] considered the cooling system' s power consumption as the sum of the fan power consumption(P_{fan}) for air cooling and the air conditioner power consumption(P_{AC}) for eliminating the heat dissipation.

$$P_{fan} = \Delta p \cdot \dot{V} \tag{10}$$

$$P_{AC} = \dot{m}_{air} C_{P,air} \Delta T_{air} \,/\, COP \tag{11}$$

In the same way as above, HVAC power consumption of each case was predicted.

The cooling system' s coefficient of performance(COP) was assumed to be 2. Since the PCM is a refrigerant of passive cooling method, it was assumed not to consume any power.

Firstly, the fan power consumption(P_{fan}) obtained through this evaluation method is presented in Table 12.

Table 12 Fan power consumption

Case / Time : 0−3,600 s	PCM 0%	PCM 16%	PCM 20%	PCM 28%	PCM 52%
Pressure drop, Δp (Pa)	377.4	379.0	379.5	380.2	383.8
Flow rate, $\dot{V}$ (m^3/s)	8.44×10^{-4}	7.18×10^{-4}	6.84×10^{-4}	6.16×10^{-4}	4.14×10^{-4}
Fan power consumption, P_{fan} (W)	0.32	0.27	0.26	0.23	0.16

The Air temperature increase(ΔT_{air}) of the inlet and outlet in the interval of 0 to 120 seconds is shown as Figure 3.10, and the Air temperature increase(ΔT_{air}) in the interval of 120 to 3,600 seconds was estimated(extrapolation) using a fitted logarithmic equation obtained through nonlinear regression analysis based on the Air temperature increase(ΔT_{air}) in the interval of 105 to 120 seconds, as shown in Table 13, Figure 3.11.

Consequently, the estimated total power consumption for the entire cycle is shown in Figure 3.12, Figure 3.13.

By applying the PCM, it was confirmed that the power consumption is lowered compared to air cooling(PCM 0% case), and higher PCM content resulted in a lower total power consumption. This phenomenon is considered that the cooling system' s thermal storage and heat capacity are both increased by a higher PCM content, reducing the amount of dissipated heat that needs to be eliminated and thus reducing power consumption.

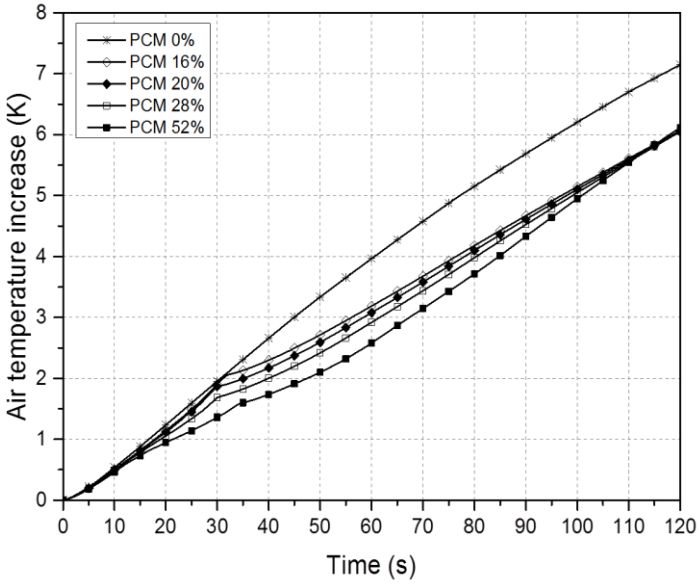

Figure 3.10 Air temperature increase behavior(time : 0−120 s)

Table 13 Estimated equations for Air temperature increase(time : 120−3,600 s)

Case	Estimated regression equation	Coefficient of determination
PCM 0%	ΔT_{air} = 11.173 × ln(time) + 263.144	0.9999
PCM 16%	ΔT_{air} = 10.154 × ln(time) + 265.975	
PCM 20%	ΔT_{air} = 10.299 × ln(time) + 265.196	
PCM 28%	ΔT_{air} = 10.553 × ln(time) + 263.892	
PCM 52%	ΔT_{air} = 11.244 × ln(time) + 260.460	

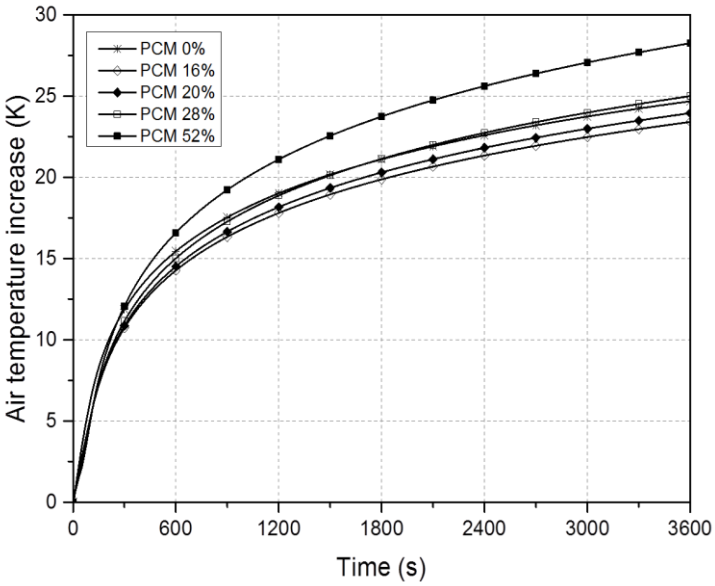

Figure 3.11 Air temperature increase behavior(time : 0−3,600 s)

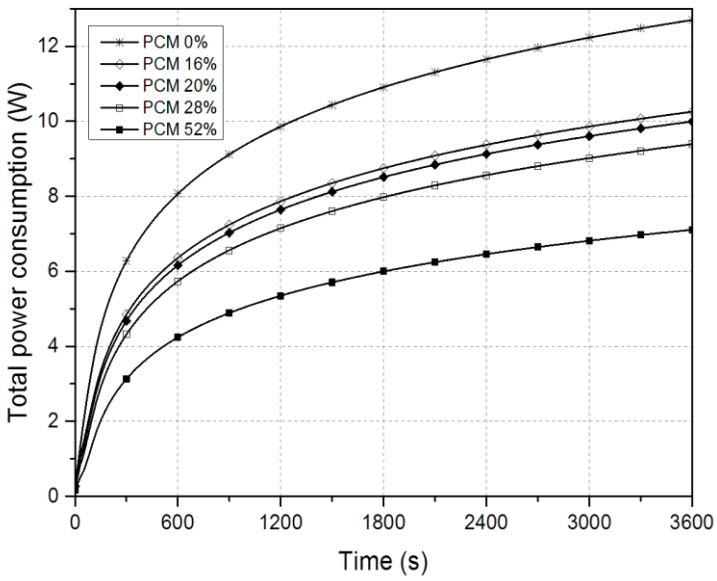

Figure 3.12 Total power consumption behavior(time : 0−3,600 s)

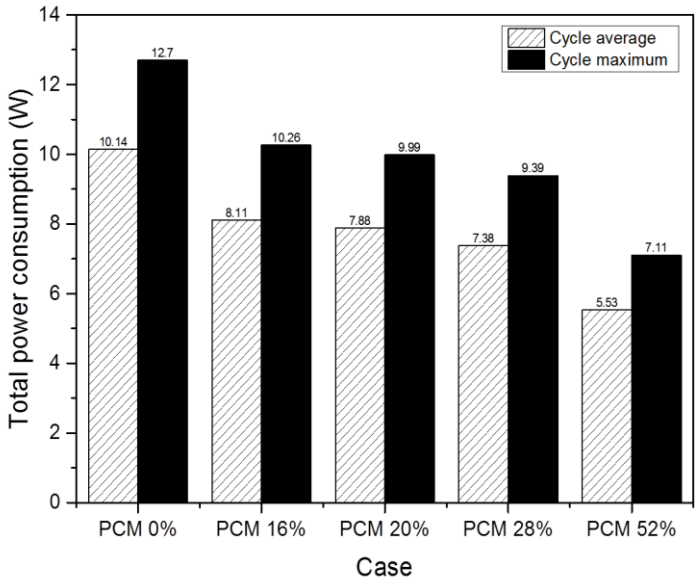

Figure 3.13 Cycle average and maximum total power consumption(time : 0-3,600 s)

3.2. Discussion

In several aspects, the application of PCM exhibited advantages in battery cooling compared to pure air cooling. However, the trends of results may differ from those observed in this study depending on factors such as level of battery heat generation, PCM phase transition temperature, practical thermal conductivity of PCM, contact resistance between elements, ambient temperature, applied air cooling specification, and others. Additionally, there are also concerns about prolonged recycling time and significant power consumption that may be required for PCM.

However, cooling through the optimal combination of PCM and air cooling is expected to reduce peak loads, leading to an enhancement in battery quality, and ensure safe management of the battery. Furthermore, it may lead to an improvement in marketability by reducing the costs of equipment for removing the dissipated heat loads.

Chapter 4. Conclusion

In this study, battery cell cooling was progressed through the latent heat absorption of PCM for about 63 to 91 seconds, depending on the PCM content. Compared to the continuous heat generation occurring during the cycle(3,600 seconds), the PCM melted completely within a short period. Therefore, combination with air cooling is considered necessary to pursue the PCM recycling and prevent deterioration of heat dissipation performance.

At the beginning of the cycle, when the PCM melting occurs, there is an observed tendency of lower cell temperatures with increasing PCM content. This tendency is attributed to the PCM's rapid heat dissipation capability, phase transition characteristic(latent heat absorption), and relatively higher heat capacity. However, after the PCM was completely melted, the Cell temperature increased more in cases with a higher PCM content, except for air cooling case. Consequently, in the PCM 16% case, the cycle average and maximum Cell temperature were the lowest, exhibiting the most superior heat dissipation performance.

The Cell temperature deviation frequently changed its ranking among the cases during the 0 to 120 seconds. Each case shows an inflection point in the trend of Cell temperature deviation near the time when PCM is completely melted. After the inflection point, the increase in Cell temperature deviation was smaller in cases with a higher PCM content. This phenomenon is considered as a consequence of the rapid heat diffusion through conduction with a higher PCM content, resulting in reduction in spatial temperature imbalances.

During the cycle, there was a tendency for the total power consumption of the cooling system to decrease as the PCM content increased. This phenomenon is considered that the cooling system’s thermal storage and heat capacity are both increased by a higher PCM content, reducing the amount of dissipated heat that needs to be eliminated and thus reducing power consumption.

Both the fan power consumption and the air conditioner power consumption were highest in the air cooling case, indicating that the application of PCM had advantages in terms of operational costs.

While confirming the potential for improving battery cooling efficiency through the utilization of PCM, it should be noted that the findings of this study may not represent all possible scenarios comprehensively.

Investigation of optimal PCM utilization for cooling system remains a task for future research, requiring thorough consideration and meticulous examination of various variables.

Bibliography

[1] Etacheri, V., Marom, R., Elazari, R., Salitra, G., & Aurbach, D. (2011). Challenges in the development of advanced Li-ion batteries: a review. Energy & Environmental Science, 4(9), 3243-3262.

[2] Nazari, A., & Farhad, S. (2017). Heat generation in lithium-ion batteries with different nominal capacities and chemistries. Applied Thermal Engineering, 125, 1501-1517.

[3] Lai, Y., Du, S., Ai, L., Ai, L., Cheng, Y., Tang, Y., & Jia, M. (2015). Insight into heat generation of lithium ion batteries based on the electrochemical-thermal model at high discharge rates. International Journal of Hydrogen Energy, 40(38), 13039-13049.

[4] Selman, J. R., Al Hallaj, S., Uchida, I., & Hirano, Y. (2001). Cooperative research on safety fundamentals of lithium batteries. Journal of power sources, 97, 726-732.

[5] Wang, J., Purewal, J., Liu, P., Hicks-Garner, J., Soukazian, S., Sherman, E., ... & Verbrugge, M. W. (2014). Degradation of lithium ion batteries employing graphite negatives and nickel–cobalt–manganese oxide+ spinel manganese oxide positives: Part 1, aging mechanisms and life estimation. Journal of Power Sources, 269, 937-948.

[6] Wen, J., Yu, Y., & Chen, C. (2012). A review on lithium-ion batteries safety issues: existing problems and possible solutions. Materials express, 2(3), 197-212.

[7] Kim, G. H., Pesaran, A., & Smith, K. (2008). Thermal Abuse Modeling of Li-Ion Cells and Propagation in Modules (Presentation) (No. NREL/PR-540-43186). National Renewable Energy Lab.(NREL), Golden, CO (United States).

[8] Jhu, C. Y., Wang, Y. W., Shu, C. M., Chang, J. C., & Wu, H. C. (2011). Thermal explosion hazards on 18650 lithium ion batteries with a VSP2 adiabatic calorimeter. Journal of hazardous materials, 192(1), 99-107.

[9] Ribière, P., Grugeon, S., Morcrette, M., Boyanov, S., Laruelle, S., & Marlair, G. (2012). Investigation on the fire-induced hazards of Li-ion battery cells by fire calorimetry. Energy & Environmental Science, 5(1), 5271-5280.

[10] UL LLC (2019, March). UL9540A Test Method for Evaluating Thermal Runaway Fire Propagation in Battery Energy Storage Systems; Module Level Test Report.

[11] Kizilel, R., Sabbah, R., Selman, J. R., & Al-Hallaj, S. (2009). An alternative cooling system to enhance the safety of Li-ion battery packs. Journal of Power Sources, 194(2), 1105-1112.

[12] Kizilel, R., Lateef, A., Sabbah, R., Farid, M. M., Selman, J. R., & Al-Hallaj, S. (2008). Passive control of temperature excursion and uniformity in high-energy Li-ion battery packs at high current and ambient temperature. Journal of Power Sources, 183(1), 370-375.

[13] Sabbah, R., Kizilel, R., Selman, J. R., & Al-Hallaj, S. (2008). Active (air-cooled) vs. passive (phase change material) thermal management of high power lithium-ion packs: Limitation of temperature rise and uniformity of temperature distribution. Journal of power sources, 182(2), 630-638.

[14] Chen, F., Huang, R., Wang, C., Yu, X., Liu, H., Wu, Q., ... & Bhagat, R. (2020). Air and PCM cooling for battery thermal management considering battery cycle life. Applied Thermal Engineering, 173, 115154.

[15] Li, Q., Cho, J. R., & Zhai, J. (2021). Optimization of thermal management system with water and phase change material cooling for Li-ion battery pack. Energies, 14(17), 5312.

[16] Ling, Z., Cao, J., Zhang, W., Zhang, Z., Fang, X., & Gao, X. (2018). Compact liquid cooling strategy with phase change materials for Li-ion batteries optimized using response surface methodology. Applied Energy, 228, 777-788.

[17] Tran, T. H., Harmand, S., Desmet, B., & Filangi, S. (2014). Experimental investigation on the feasibility of heat pipe cooling for HEV/EV lithium-ion battery. Applied Thermal Engineering, 63(2), 551-558.

[18] Akbarzadeh, M., Kalogiannis, T., Jaguemont, J., Jin, L., Behi, H., Karimi, D., ... & Berecibar, M. (2021). A comparative study between air cooling and liquid cooling thermal management systems for a high-energy lithium-ion battery module. Applied Thermal Engineering, 198, 117503.

[19] Chen, D., Jiang, J., Kim, G. H., Yang, C., & Pesaran, A. (2016). Comparison of different cooling methods for lithium ion battery cells. Applied Thermal Engineering, 94, 846-854.

[20] LG Chem ESS Battery Division Catalog (2018, August). CHANGE YOUR ENERGY CHARGE YOUR LIFE.

[21] Ma, S., Jiang, M., Tao, P., Song, C., Wu, J., Wang, J., ... & Shang, W. (2018). Temperature effect and thermal impact in lithium-ion batteries: A review. Progress in Natural Science: Materials International, 28(6), 653-666.

[22] Winstead, C., Bhandari, M., Nutaro, J., & Kuruganti, T. (2020). Peak load reduction and load shaping in HVAC and refrigeration systems in commercial buildings by using a novel lightweight dynamic priority-based control strategy. Applied Energy, 277, 115543.

[23] Song, L., Zhang, H., & Yang, C. (2019). Thermal analysis of conjugated cooling configurations using phase change material and liquid cooling techniques for a battery module. International Journal of Heat and Mass Transfer, 133, 827-841.

[24] Huang, R., Li, Z., Hong, W., Wu, Q., & Yu, X. (2020). Experimental and numerical study of PCM thermophysical parameters on lithium-ion battery thermal management. Energy Reports, 6, 8-19.

[25] Somasundaram, K., Birgersson, E., & Mujumdar, A. S. (2012). Thermal–electrochemical model for passive thermal management of a spiral-wound lithium-ion battery. Journal of Power Sources, 203, 84-96.

[26] Zhao, Y., Zou, B., Li, C., & Ding, Y. (2019). Active cooling based battery thermal management using composite phase change materials. Energy Procedia, 158, 4933-4940.

[27] Al-Hallaj, S., Kizilel, R., Lateef, A., Sabbah, R., Farid, M., & Selman, J. R. (2005, September). Passive thermal management using phase change material (PCM) for EV and HEV Li-ion batteries. In 2005 IEEE vehicle power and propulsion conference (pp. 5-pp). IEEE.

[28] Alhusseny, A., Al-Zurfi, N., Nasser, A., Al-Fatlawi, A., & Aljanabi, M. (2020). Impact of using a PCM-metal foam composite on charging/discharging process of bundled-tube LHTES units. International Journal of Heat and Mass Transfer, 150, 119320.

[29] Cui, H. T. (2012). Experimental investigation on the heat charging process by paraffin filled with high porosity copper foam. Applied thermal engineering, 39, 26-28.

[30] Babapoor, A., Azizi, M., & Karimi, G. (2015). Thermal management of a Li-ion battery using carbon fiber-PCM composites. Applied Thermal Engineering, 82, 281-290.

[31] Brent, A. D., Voller, V. R., & Reid, K. T. J. (1988). Enthalpy-porosity technique for modeling convection-diffusion phase change: application to the melting of a pure metal. Numerical Heat Transfer, Part A Applications, 13(3), 297-318.

[32] Voller, V. R., Cross, M., & Markatos, N. C. (1987). An enthalpy method for convection/diffusion phase change. International journal for numerical methods in engineering, 24(1), 271-284.

[33] SIEMENS. Simcenter STAR-CCM+ User Guide, Version 13.04.

[34] C. Bojanowski, A. Bergeron, J. Licht. (2020). Involute Working Group-Validation of CFD Turbulence Models for Steady-State Safety Analysis, Nuclear Science & Engineering Division, Argonne National Laboratory

[35] Hong, S. W., Lee, Y. T., & Chung, J. D. (2015). Restrictions on the analytic approach of unconstrained melting inside a spherical capsule. Journal of Mechanical Science and Technology, 29, 5035-5042.

[36] Tan, F. L. (2008). Constrained and unconstrained melting inside a sphere. International Communications in Heat and Mass Transfer, 35(4), 466-475.

[37] Dhaidan, N. S., & Khodadadi, J. M. (2015). Melting and convection of phase change materials in different shape containers: A review. Renewable and Sustainable Energy Reviews, 43, 449-477.

국문 초록

본 연구에서는 상변화물질(PCM)을 적용한 배터리 냉각시스템의 적절성 및 최적안을 고찰하였다. 중대형 배터리로서의 활용이 대두되는 파우치형 배터리 셀에 대한 냉각을 3차원 경계조건 및 실제 시스템의 체적을 유지하는 제한 내에서 연구를 진행한 의의가 있다.

순수 공냉(PCM 0% case)부터 공냉과 PCM의 하이브리드 냉각(PCM 16%, PCM 20%, PCM 28%, PCM 52% case) 및 순수 PCM 냉각(PCM 100% case)을 추구하는 각 Case를 독립변수로서 냉각 성능, 냉각 균일성, 소비전력 등을 비교 분석해보았다.

상변화 문제에 있어 상경계면에서의 열평형 방정식과 급변하는 점성, 밀도 등의 물리량은 수치해석 시 잔차 수렴성에 어려움을 주므로 적절 time step, 격자 크기, 상변화 거동 관련 매개변수를 선정하였고 잔차의 최소 기준을 준수하여 해석에 신뢰성을 부여 및 PCM의 융해 거동을 정확히 예측하는 데에 있어 구현되어야 할 중요한 물리적 현상인 Unconstrained melting 효과를 수치해석적으로 확인하였다.

PCM의 융해가 일어나는 구간에서는 PCM의 함량이 높을수록 전도를 통한 빠른 열전달, 상변화 시 잠열 흡수 및 열용량이 큰 특성으로 인해 대류를 통한 냉각이 지배적인 공냉(PCM 0% case)보다 냉각 성능이 우수하였다. PCM의 융해가 완전히 종료된 후에는 PCM 16% case에서 Cell 냉각 성능이 가장 우수하였으며 결과적으로 Cell 온도의 사이클 전체적인 평균값과 최대값 또한 PCM 16% case에서 가장 낮게 관측되었다.

PCM의 적용은 PCM의 융해 구간 및 융해 이후의 구간에서 각각 공냉 대비 낮은 Cell 온도편차와 Cell 온도편차 상승률을 보여 적용의 이점을 갖았다.

또, PCM의 적용은 공냉 대비 소비전력 측면에서도 우위를 갖음을 확인할 수 있었다.

주요어 : 배터리 냉각, 상변화물질(수동 냉각), 공냉(능동 냉각), 비구속조건 융해, 수치 해석

학번 : 2021-28582